

Fermionic decay of charged Higgs boson in low mass region in Georgi Machacek Model

Swagata Ghosh^{a,b,c*}

^a *Department of Physics and Astrophysics, University of Delhi, Delhi, India.*

^b *Department of Physics, SGTB Khalsa College, University of Delhi, Delhi, India.*

^c *Department of Physics, Indian Institute of Technology Kharagpur, Kharagpur 721302, India.*

Abstract

At the Large Hadron Collider (LHC), ATLAS and CMS collaborations observed various decay modes of the light charged Higgs bosons produced by top (anti)quark decays. In this paper, we are interested in the subsequent decay of the light charged Higgs boson into a charm and a strange quark-antiquark pair and into a tau and a tau-neutrino pair, separately, in the context of the Georgi-Machacek model, which offers a large triplet vacuum expectation value (vev) preserving custodial symmetry. We show that these experimental observations constrain the triplet vev from above. We explore the model parameter space consistent with the theoretical constraints, the latest Higgs data and the experimental data for light charged Higgs decaying to cs and $\tau\nu_\tau$.

1 Introduction

The discovery of the Higgs boson with a mass around 125 GeV at the Large Hadron Collider (LHC) experiment [1, 2] in the year of 2012 let the Standard Model (SM) have great success. The possibility of having new exotic particles still cannot be thrown away. It is always possible that the discovered 125 GeV scalar resonance is a part of a non-minimal Higgs sector accommodating one or more non-standard scalar multiplets. Besides, the new beyond Standard Model (BSM) scalar can be neutral or charged.

With an appealing phenomenology, the physical charged scalars got searched at LHC prolongedly. These charged scalars can be lighter as well as heavier than the top quark mass (m_t). At LHC, light charged scalar decaying to cb [3, 4], cs [5, 7, 8], and $\tau\nu_\tau$ [10–16] is searched. Besides, light charged scalars decay in different multi-Higgs doublet models [17, 19–23] and in other colliders [24–26] are also searched and studied.

Most of the BSM models with extended scalar sectors commit singly charged scalar particle, through which one can explore the model parameter space. In this paper, we consider the Georgi-Machacek (GM) Model [27], where both of the singly and doubly charged scalars are present, though we focus only on the decay of the singly charged scalar when its mass is in the range of 80-160 GeV.

The GM model is atypical of the other triplet extensions of the SM as it preserves the custodial symmetry in the tree level, i.e., the ρ -parameter is equal to unity in this model, hence resulting in a sizeable triplet vacuum expectation value (VEV), v_2 . In the GM model, the extended scalar sector contains one real triplet and one complex triplet, neutral components of both possessing the same VEV. The physical scalar sector includes ten scalars ordered as two singlets, one triplet, and one quintuplet. Out of these ten scalars, 4 scalars are charge-neutral (h, H, H_3^0, H_5^0), another 4 are singly-charged (H_3^\pm, H_5^\pm), and the rest 2 scalars are doubly-charged ($H_5^{\pm\pm}$). The two singly-charged scalars H_5^\pm do not couple to the SM fermions, whereas, the other two singly-charged scalars H_3^\pm couple to the SM fermions, and the strength of coupling is directly proportional to the triplet VEV v_2 , which is sizeable enough in the GM model. We will focus on the decay of the H_3^\pm in this paper.

Decay of charged scalar, heavier than the top quark mass, is studied in the context of the Georgi-Machacek model [28, 29]. The theoretical limits [30–34] on the Lagrangian parameters, the indirect constraints [35], Higgs boson pair productions at the LHC [36], electroweak phase transition [37, 38], impacts of higher dimensional operators [39] in the Georgi-Machacek model are well scrutinized. For

*swgtghsh54@gmail.com

phenomenological studies of this model at the LHC [40], electron-positron collider [41], the reader may also consult the literature. There are also some variants of the GM model [42, 43]. One can scan the parameter space of this model using the calculator [44]. For the global fits in the GM model, see [45]. It is to be mentioned here that, inspite of the extensive phenomenological study of the GM model, the exploration of the parameter space in case of the light charged scalar together with the LHC data has not been examined as yet.

This paper is organized as follows. In Sec. 2 we describe the model in brief. We enlist the theoretical constraints and LHC data, with their effects on the parameter space of the GM model in Sec. 3. The results are given in Sec. 4. Finally we conclude in Sec. 5.

2 The Georgi-Machacek Model

One $SU(2)_L$ real triplet $(\xi^+, \xi^0, \xi^-)^T$ with hypercharge $Y = 0$ and one $SU(2)_L$ complex triplet $(\chi^{++}, \chi^+, \chi^0)^T$ with $Y = 2$ are appended to the particle contents of the scalar sector of the Standard Model to obtain the Georgi-Machacek model. We mostly persue the notations followed in [31] throughout this paper.

The SM doublet $(\phi^+, \phi^0)^T$ with $Y = 1$ and the non-standard triplets can be expressed in terms of bi-doublet and bi-triplet respectively, as,

$$\Phi = \begin{pmatrix} \phi^{0*} & \phi^+ \\ \phi^- & \phi^0 \end{pmatrix}, \quad X = \begin{pmatrix} \chi^{0*} & \xi^+ & \chi^{++} \\ \chi^- & \xi^0 & \chi^+ \\ \chi^{--} & \xi^- & \chi^0 \end{pmatrix}. \quad (1)$$

The most general scalar potential is given by,

$$\begin{aligned} V(\Phi, X) = & \frac{\mu_2^2}{2} \text{Tr}(\Phi^\dagger \Phi) + \frac{\mu_3^2}{2} \text{Tr}(X^\dagger X) + \lambda_1 [\text{Tr}(\Phi^\dagger \Phi)]^2 + \lambda_2 \text{Tr}(\Phi^\dagger \Phi) \text{Tr}(X^\dagger X) \\ & + \lambda_3 \text{Tr}(X^\dagger X X^\dagger X) + \lambda_4 [\text{Tr}(X^\dagger X)]^2 - \lambda_5 \text{Tr}(\Phi^\dagger \tau^a \Phi \tau^b) \text{Tr}(X^\dagger t^a X t^b) \\ & - M_1 \text{Tr}(\Phi^\dagger \tau^a \Phi \tau^b) (UXU^\dagger)_{ab} - M_2 \text{Tr}(X^\dagger t^a X t^b) (UXU^\dagger)_{ab}, \end{aligned} \quad (2)$$

with $\tau^a = \sigma^a/2$, where σ^a are the three Pauli matrices, and the t^a s as,

$$t^1 = \frac{1}{\sqrt{2}} \begin{pmatrix} 0 & 1 & 0 \\ 1 & 0 & 1 \\ 0 & 1 & 0 \end{pmatrix}, \quad t^2 = \frac{1}{\sqrt{2}} \begin{pmatrix} 0 & -i & 0 \\ i & 0 & -i \\ 0 & i & 0 \end{pmatrix}, \quad t^3 = \begin{pmatrix} 1 & 0 & 0 \\ 0 & 0 & 0 \\ 0 & 0 & -1 \end{pmatrix}. \quad (3)$$

The matrix U in the trilinear terms of the GM potential is given by,

$$U = \frac{1}{\sqrt{2}} \begin{pmatrix} -1 & 0 & 1 \\ -i & 0 & -i \\ 0 & \sqrt{2} & 0 \end{pmatrix}. \quad (4)$$

After the electroweak symmetry breaking (EWSB), the neutral components of the bi-doublet and the bi-triplet acquire the VEVs, as,

$$\langle \phi^0 \rangle = \frac{v_1}{\sqrt{2}}, \quad \langle \chi^0 \rangle = \langle \xi^0 \rangle = v_2. \quad (5)$$

Note that, the equality of the real and complex triplet VEVs corresponds to the preservation of the custodial symmetry of the potential at the tree level leading to $\rho_{\text{tree}} \equiv M_W^2/M_Z^2 \cos^2 \theta_W = 1$.

The EW VEV v relates to the doublet and triplet VEVs as,

$$\sqrt{v_1^2 + 8v_2^2} = v \approx 246 \text{ GeV}. \quad (6)$$

The doublet-triplet mixing angle may be expressed as,

$$\tan \beta = \frac{2\sqrt{2}v_2}{v_1}, \quad (7)$$

In terms of VEVs given in Eq. (5), the potential (2) becomes

$$\begin{aligned} V(v_1, v_2) = & \frac{\mu_2^2}{2}v_1^2 + 3\frac{\mu_3^2}{2}v_2^2 + \lambda_1 v_1^4 + \frac{3}{2}(2\lambda_2 - \lambda_5)v_1^2 v_2^2 \\ & + 3(\lambda_3 + 3\lambda_4)v_2^4 - \frac{3}{4}M_1 v_1^2 v_2 - 6M_2 v_2^3, \end{aligned} \quad (8)$$

Hence, using the extremisation conditions one can easily extract the bilinear coefficients of the potential as,

$$\begin{aligned} \mu_2^2 = & -4\lambda_1 v_1^2 - 3(2\lambda_2 - \lambda_5)v_2^2 + \frac{3}{2}M_1 v_2, \\ \mu_3^2 = & -(2\lambda_2 - \lambda_5)v_1^2 - 4(\lambda_3 + 3\lambda_4)v_2^2 + \frac{M_1 v_1^2}{4v_2} + 6M_2 v_2. \end{aligned} \quad (9)$$

The scalar sector of the GM model consists of ten physical fields of which five are part of a custodial quintuplet $H_5 = (H_5^{++}, H_5^+, H_5^0, H_5^-, H_5^{--})^T$, three are part of a custodial triplet $H_3 = (H_3^+, H_3^0, H_3^-)^T$, and the rest two are custodial singlets H_1^0 and $H_1^{0'}$. These ten physical fields may be expressed in terms of the component fields and the angle β as,

$$\begin{aligned} H_5^{++} = \chi^{++}, \quad H_5^+ = \frac{(\chi^+ - \xi^+)}{\sqrt{2}}, \quad H_5^0 = \sqrt{\frac{2}{3}}\xi^0 - \sqrt{\frac{1}{3}}\chi^{0R}, \\ H_3^+ = -\sin \beta \phi^+ + \cos \beta \frac{(\chi^+ + \xi^+)}{\sqrt{2}}, \quad H_3^0 = -\sin \beta \phi^{0I} + \cos \beta \chi^{0I}, \\ H_1^0 = \phi^{0R}, \quad H_1^{0'} = \sqrt{\frac{1}{3}}\xi^0 + \sqrt{\frac{2}{3}}\chi^{0R}. \end{aligned} \quad (10)$$

The physical fields of the multiplets are mass degenerate. The square of the common mass of the quintuplet H_5 and the triplet H_3 are given by,

$$\begin{aligned} m_5^2 = & \frac{M_1}{4v_2}v_1^2 + 12M_2 v_2 + \frac{3}{2}\lambda_5 v_1^2 + 8\lambda_3 v_2^2, \\ m_3^2 = & \left(\frac{M_1}{4v_2} + \frac{\lambda_5}{2} \right) v^2, \end{aligned} \quad (11)$$

respectively.

The custodial singlets H_1^0 and $H_1^{0'}$ mix to yield the mass eigenstates h and H as,

$$\begin{aligned} h &= \cos \alpha H_1^0 - \sin \alpha H_1^{0'}, \\ H &= \sin \alpha H_1^0 + \cos \alpha H_1^{0'}, \end{aligned} \quad (12)$$

with the mass squared matrix

$$\mathcal{M}^2 = \begin{pmatrix} \mathcal{M}_{11}^2 & \mathcal{M}_{12}^2 \\ \mathcal{M}_{21}^2 & \mathcal{M}_{22}^2 \end{pmatrix}, \quad (13)$$

where

$$\begin{aligned} \mathcal{M}_{11}^2 &= 8\lambda_1 v_1^2, \\ \mathcal{M}_{12}^2 &= \mathcal{M}_{21}^2 = \frac{\sqrt{3}}{2} [-M_1 + 4(2\lambda_2 - \lambda_5)v_2] v_1, \\ \mathcal{M}_{22}^2 &= \frac{M_1 v_1^2}{4v_2} - 6M_2 v_2 + 8(\lambda_3 + 3\lambda_4)v_2^2. \end{aligned} \quad (14)$$

The neutral scalar mixing angle α can be parametrised in terms of the components of the mass-squared matrix as,

$$\tan 2\alpha = \frac{2\mathcal{M}_{12}^2}{\mathcal{M}_{22}^2 - \mathcal{M}_{11}^2}. \quad (15)$$

The mass-squared of the physical neutral scalars are,

$$m_{h,H}^2 = \frac{1}{2} \left[\mathcal{M}_{11}^2 + \mathcal{M}_{22}^2 \mp \sqrt{(\mathcal{M}_{11}^2 - \mathcal{M}_{22}^2)^2 + 4(\mathcal{M}_{12}^2)^2} \right]. \quad (16)$$

We assume here that $m_H > m_h$ and consider the CP-even neutral scalar with smaller mass as the SM-like Higgs boson, such that $m_h \approx 125$ GeV.

The bilinear couplings (μ_2^2 and μ_3^2) present in the scalar potential are already traded in terms of the VEVs v_1 and v_2 in the Eq. (9). The quartic couplings λ_i ($i = 1$ to 5) in the potential (2) can be expressed in terms of the four physical masses, m_h , m_H , m_3 , m_5 , and the mixing angle α as,

$$\begin{aligned} \lambda_1 &= \frac{1}{8v_1^2} (m_h^2 \cos^2 \alpha + m_H^2 \sin^2 \alpha), \\ \lambda_2 &= \frac{1}{8v_2} \left[(m_H^2 - m_h^2) \frac{1}{\sqrt{3}v_1} \sin 2\alpha - M_1 + 8m_3^2 \frac{v_2}{v^2} \right], \\ \lambda_3 &= \frac{1}{8v_2^2} \left(m_5^2 - 3m_3^2 \frac{v_1^2}{v^2} + \frac{M_1 v_1^2}{2v_2} - 12M_2 v_2 \right), \\ \lambda_4 &= \frac{1}{24v_2^2} \left(m_h^2 \sin^2 \alpha + m_H^2 \cos^2 \alpha - m_5^2 + 3m_3^2 \frac{v_1^2}{v^2} - 3M_1 \frac{v_1^2}{4v_2} + 18M_2 v_2 \right), \\ \lambda_5 &= 2 \left(\frac{m_3^2}{v^2} - \frac{M_1}{4v_2} \right). \end{aligned} \quad (17)$$

3 Theoretical constraints and LHC data

The theoretical constraints, mainly resulting from the perturbative unitarity and electroweak vacuum stability, and the experimental constraints, typically following the LHC data put the limit on the parameters of the GM potential. Here, we write down the theoretical constraints already available in the literature. The reader may follow [31, 35] for the detailed knowledges of the theoretical constraints.

Constraints obtained from perturbative unitarity are given by,

$$\begin{aligned} \sqrt{(6\lambda_1 - 7\lambda_3 - 11\lambda_4)^2 + 36\lambda_2^2} + |6\lambda_1 + 7\lambda_3 + 11\lambda_4| &< 4\pi, \\ \sqrt{(2\lambda_1 + \lambda_3 - 2\lambda_4)^2 + \lambda_5^2} + |2\lambda_1 - \lambda_3 + 2\lambda_4| &< 4\pi, \\ |2\lambda_3 + \lambda_4| &< \pi, \\ |\lambda_2 - \lambda_5| &< 2\pi, \end{aligned} \quad (18)$$

and the constraints obtained from electroweak vacuum stability are given by,

$$\begin{aligned} \lambda_1 &> 0, \\ \lambda_2 + \lambda_3 &> 0, \\ \lambda_2 + \frac{1}{2}\lambda_3 &> 0, \\ -|\lambda_4| + 2\sqrt{\lambda_1(\lambda_2 + \lambda_3)} &> 0, \\ \lambda_4 - \frac{1}{4}|\lambda_5| + \sqrt{2\lambda_1(2\lambda_2 + \lambda_3)} &> 0. \end{aligned} \quad (19)$$

For the constraints coming from the LHC data, we consider the Higgs data at $\sqrt{s} = 13$ TeV [46, 47]. Here, we contemplate the lightest CP-even scalar h as the SM-like Higgs with mass $m_h \approx 125$ GeV. Therefore, we require to know the couplings of h with the SM fermions and the vector bosons, which we enlist below :

$$g_{h\bar{f}f} = -i \frac{m_f c_\alpha}{v c_\beta}, \quad ig_{hWW}\eta_{\mu\nu} = ic_W^2 g_{hZZ}\eta_{\mu\nu} = -i \frac{e^2}{6s_W^2} (8\sqrt{3}s_\alpha v_2 - 3c_\alpha v_1)\eta_{\mu\nu}. \quad (20)$$

The ratio of the fermionic and bosonic couplings with h in the GM model to that in the SM model are given by,

$$\kappa_f^h = \frac{v}{v_1} c_\alpha, \quad \kappa_V^h = -\frac{1}{3v} (8\sqrt{3}s_\alpha v_2 - 3c_\alpha v_1). \quad (21)$$

For the decay $h \rightarrow \gamma\gamma$, the charged scalars coming from the triplet and quintuplet contribute at loop level. So, we need the corresponding couplings :

$$\begin{aligned} -ig_{hH_3^+H_3^-} &= -i(64\lambda_1 c_\alpha \frac{v_2^2 v_1}{v^2} - \frac{8}{\sqrt{3}} \frac{v_1^2 v_2}{v^2} s_\alpha (\lambda_3 + 3\lambda_4) - \frac{4}{\sqrt{3}} \frac{v_2 M_1}{v^2} (s_\alpha v_2 - \sqrt{3}c_\alpha v_1) \\ &\quad - \frac{16}{\sqrt{3}} \frac{v_2^3}{v^2} s_\alpha (6\lambda_2 + \lambda_5) - c_\alpha \frac{v_1^3}{v^2} (\lambda_5 - 4\lambda_2) + 2\sqrt{3}M_2 \frac{v_1^2}{v^2} s_\alpha \\ &\quad - \frac{8}{\sqrt{3}} \lambda_5 \frac{v_1 v_2}{v^2} (s_\alpha v_1 - \sqrt{3}c_\alpha v_2)), \\ -ig_{hH_5^+H_5^-} &= -ig_{hH_5^{++}H_5^{--}} = -i(-8\sqrt{3}(\lambda_3 + \lambda_4)s_\alpha v_2 + (4\lambda_2 + \lambda_5)c_\alpha v_1 - 2\sqrt{3}M_2 s_\alpha). \end{aligned} \quad (22)$$

One can replace the λ_i s present in the Eq. (22) with the help of the expressions given in (17) to get the couplings in terms of the physical masses, mixing angle, VEVs, and the trilinear coefficients.

The vertices involving the charged scalar H_3^\pm and two fermions are given by :

$$\begin{aligned} H_3^+ \bar{u}d : &-i\sqrt{2} V_{ud} \tan \beta \left(\frac{m_u}{v} P_L - \frac{m_d}{v} P_R \right), & H_3^- \bar{d}u : &-i\sqrt{2} V_{ud}^* \tan \beta \left(\frac{m_u}{v} P_R - \frac{m_d}{v} P_L \right), \\ H_3^+ \bar{\nu}l : &i\sqrt{2} \tan \beta \frac{m_l}{v} P_R, & H_3^- \bar{l}\nu : &i\sqrt{2} \tan \beta \frac{m_l}{v} P_L. \end{aligned} \quad (23)$$

Here, V_{ud} is the CKM matrix element and the projection operators $P_{R,L}$ are given by $(1 \pm \gamma_5)/2$.

Considering the Eq. (9) and (17), we have nine independent parameters ($m_h, m_H, m_3, m_5, \sin \alpha, v_2, v, M_1, M_2$) and we choose m_h as identical to the SM-like Higgs mass. To scan the parameter space, we choose the mass of the heavier CP-even neutral scalar H starting from 150 GeV and that of the members of the multiplets starting from 80 GeV [18]. The upper limit of m_H and m_5 are set to 1000 GeV. We vary the triplet VEV v_2 in between 0 – 60 GeV. v is the electroweak VEV as usual. Therefore, after setting m_h and v at the fixed values, we are left with seven independent parameters. Since our purpose is to study the low mass phenomenology of H_3^+ , we consider m_3 in between 80 – 160 GeV. Finally, we consider M_1 and M_2 in between $[-1000, 1000]$ GeV.

Now, in Fig. (1) we present the plots in the $m_3 - v_2, m_5 - v_2, m_3 - m_5, m_H - v_2, v_2 - M_1, v_2 - M_2, M_1 - M_2, \sin \alpha - v_2$ plane, where the region allowed by the theoretical constraints, LHC Higgs signal data at $\sqrt{s} = 13$ TeV without considering the charged Higgs contribution in the $h \rightarrow \gamma\gamma$ decay, LHC Higgs signal data at $\sqrt{s} = 13$ TeV considering the charged Higgs contribution in the $h \rightarrow \gamma\gamma$ decay, all the above stated constraints are shown by blue, red, violet, dark-green points respectively.

First, we consider the theoretical constraints given in the Eqs. (18, 19) that restrict the quartic couplings λ_i s of the scalar potential, which are shown by the blue points in the Fig. (1). We fixed the upper limit of m_3 at 160 GeV. The expression of m_3 given in the Eq. (11) shows that this puts a limit on M_1 in turn. We varied the other trilinear co-efficient M_2 in a selected range of $[-1000, 1000]$ GeV. Also, the triplet VEV v_2 is varied between $[0, 60]$ GeV and the doublet VEV v_1 is varied accordingly (see Eq. 6). So, one can say in some sense that besides the quartic couplings λ_i s, the trilinear co-efficients $M_{1,2}$

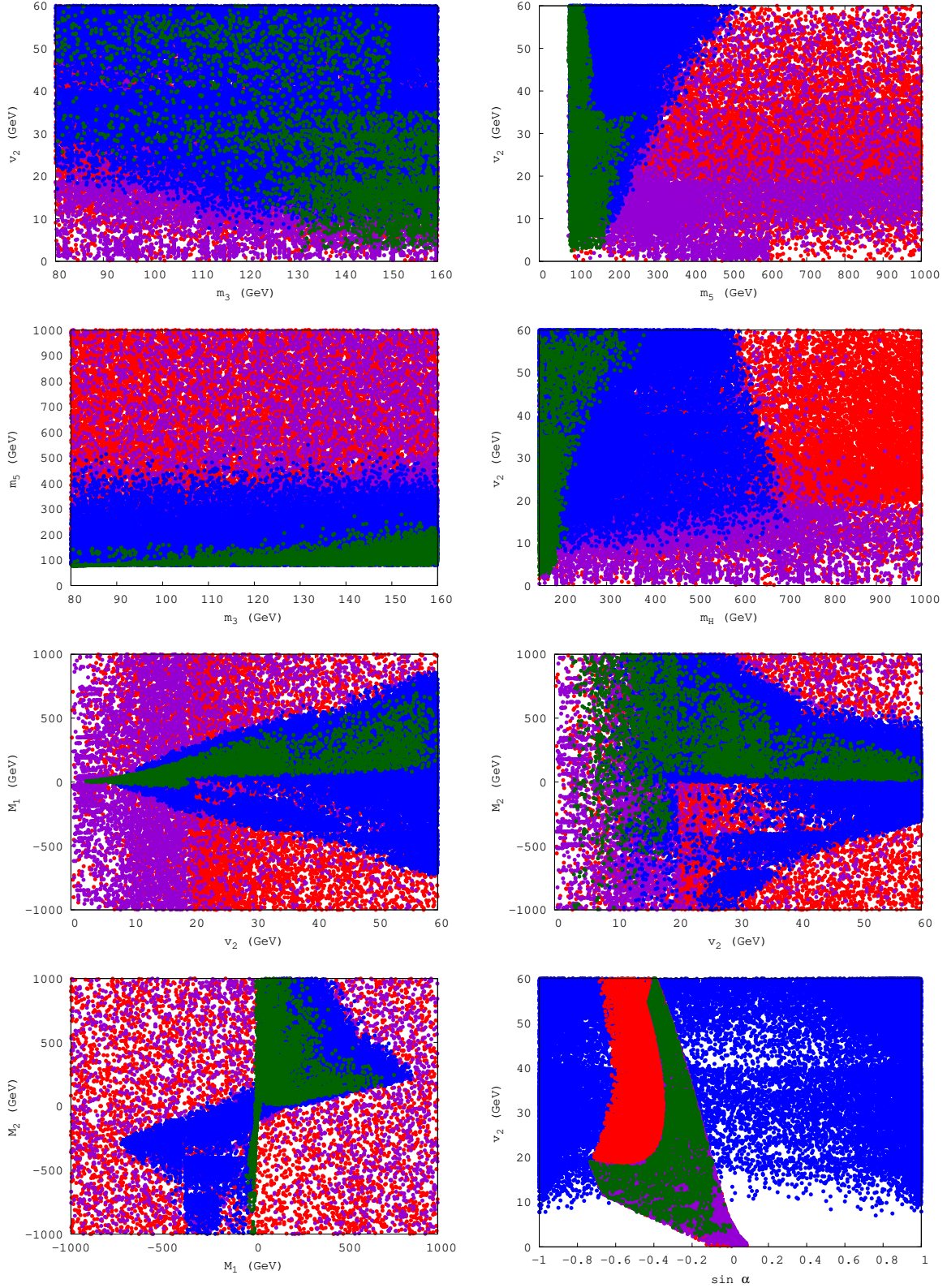


Figure 1: Allowed parameter space in the $m_3 - v_2$, $m_5 - v_2$, $m_3 - m_5$, $m_H - v_2$, $v_2 - M_1$, $v_2 - M_2$, $M_1 - M_2$, $\sin \alpha - v_2$ plane by the theoretical constraints, LHC Higgs signal data at $\sqrt{s} = 13$ TeV without considering the charged Higgs contribution in the $h \rightarrow \gamma\gamma$ decay, LHC Higgs signal data at $\sqrt{s} = 13$ TeV considering the charged Higgs contribution in the $h \rightarrow \gamma\gamma$ decay, all the above stated constraints are shown by blue, red, violet, dark-green points respectively.

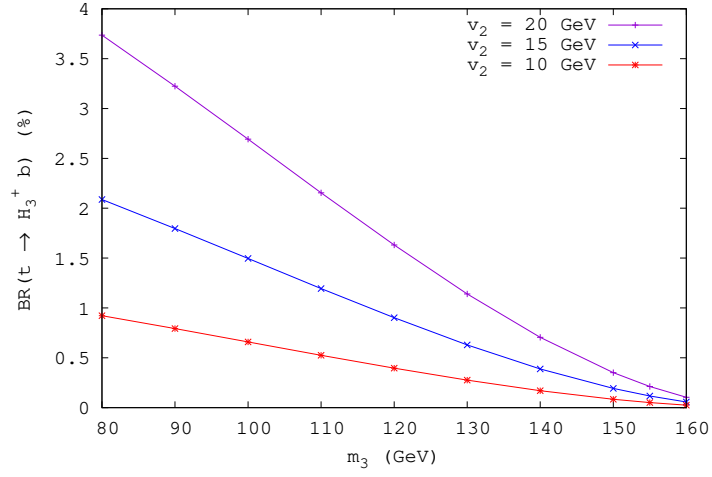


Figure 2: Branching ratio of $t \rightarrow H_3^+ b$ as a function of mass m_3 in GeV, for $v_2 = 10, 15, 20$ GeV. The other parameters chosen as mentioned in the Eq. (24).

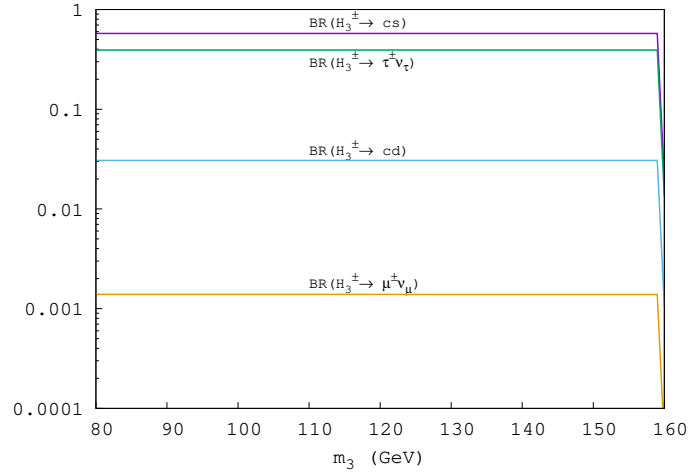


Figure 3: Branching ratios of H_3^\pm as a function of mass m_3 in GeV at $v_2 = 20$ GeV. The other independent parameters are chosen as mentioned in the Eq. (24).

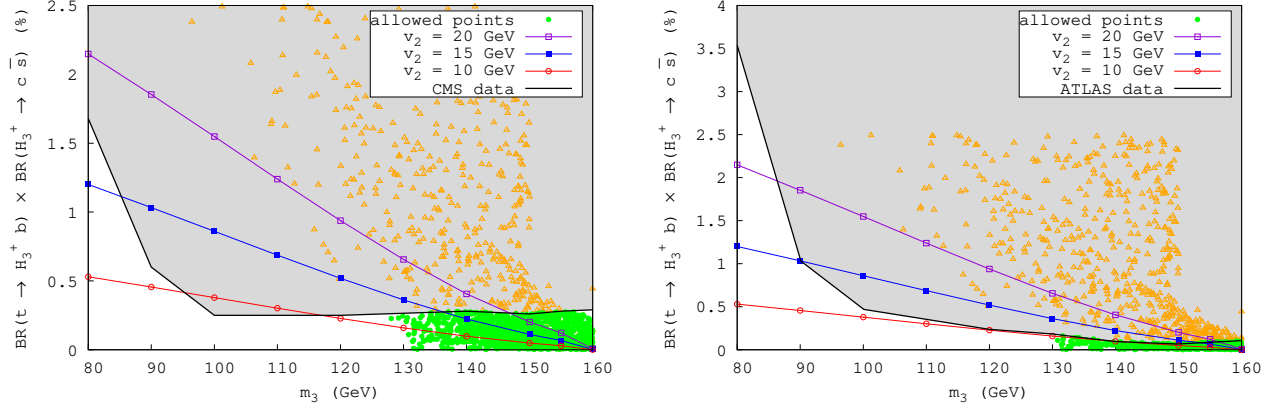


Figure 4: Branching ratio of the top quark decaying into H_3^+ and b times the branching ratio of H_3^+ decaying into c and \bar{s} as a function of mass m_3 in GeV, for $v_2 = 10, 15, 20$ GeV with red, blue and violet coloured lines respectively. The black line represents the limit from (Left) CMS experiment [5] and (Right) ATLAS experiment [6]. The shaded region is excluded by the experimental data. All the coloured points (green and orange) are allowed by the theoretical constraints. The orange and green points are forbidden and allowed by the corresponding experimental data respectively.

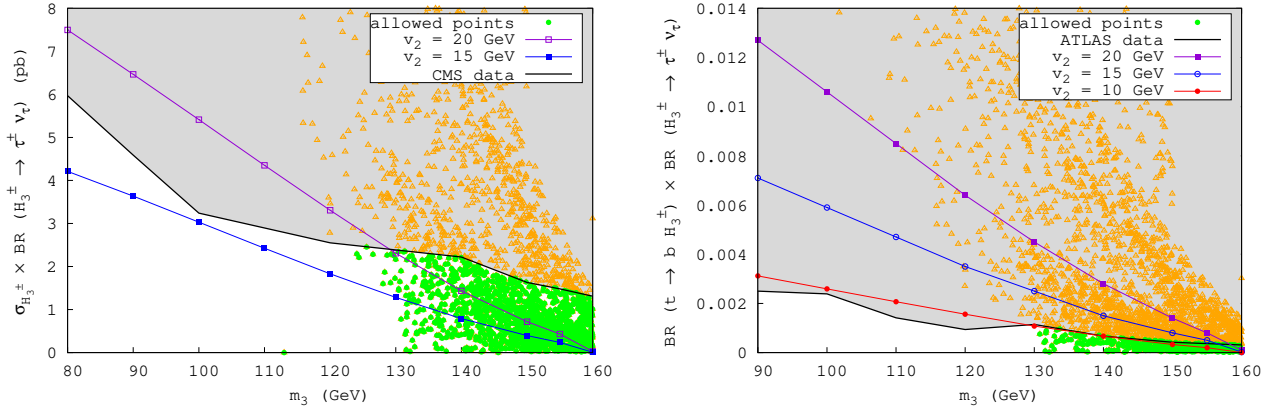


Figure 5: Left : Production cross section times branching ratio of H_3^\pm decaying into $\tau^\pm \nu_\tau$ as a function of mass m_3 in GeV, for $v_2 = 15, 20$ GeV. The black line represents the limit from CMS experiment [10]. Right : Branching ratio of the top quark decaying into H_3^\pm and b times the branching ratio of H_3^\pm decaying into $\tau^\pm \nu_\tau$ as a function of mass m_3 in GeV, for $v_2 = 10, 15, 20$ GeV. The black line represents the limit from ATLAS experiment [9].

The red, blue and violet lines correspond to $v_2 = 10, 15, 20$ GeV respectively. The shaded region is excluded by the experimental data. All the coloured points (green and orange) are allowed by the theoretical constraints. The orange and green points are forbidden and allowed by the corresponding experimental data respectively.

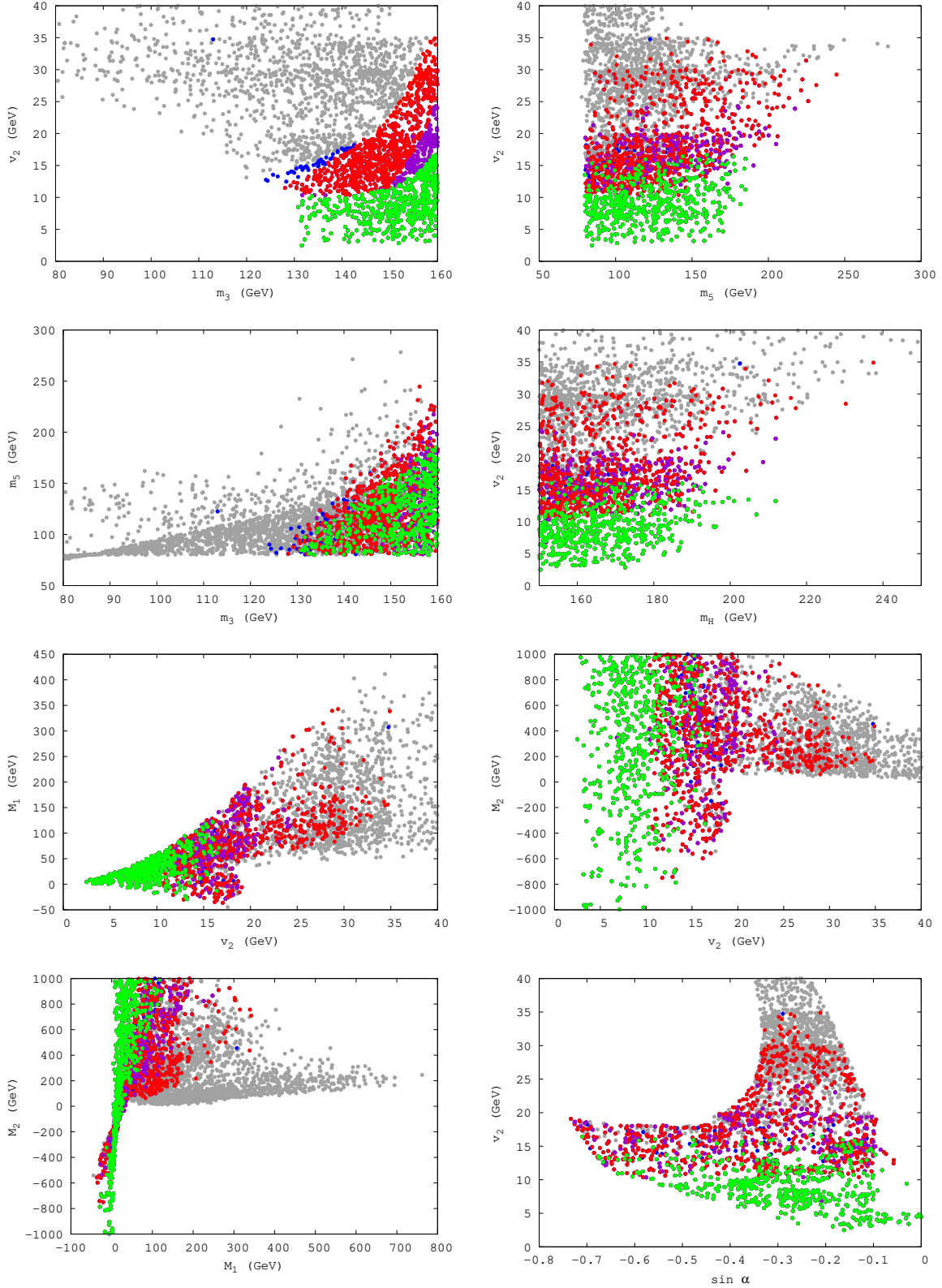


Figure 6: Allowed parameter space in the $m_3 - v_2$, $m_5 - v_2$, $m_3 - m_5$, $m_H - v_2$, $v_2 - M_1$, $v_2 - M_2$, $M_1 - M_2$, $\sin \alpha - v_2$ plane. All points are allowed from theoretical constraints as well as LHC data at $\sqrt{s} = 13$ TeV. The gray points are excluded from all the $H_3^\pm \rightarrow cs, \tau\nu$ data of CMS and ATLAS experiments. The blue points are excluded by $H_3^\pm \rightarrow \tau\nu$ ATLAS, $H_3^\pm \rightarrow cs$ CMS as well as ATLAS data. The red points are excluded by $H_3^\pm \rightarrow cs, \tau\nu$ ATLAS data. The violet points are excluded by $H_3^\pm \rightarrow \tau\nu$ ATLAS data. The green points are allowed by all the $H_3^\pm \rightarrow cs, \tau\nu$ CMS and ATLAS data.

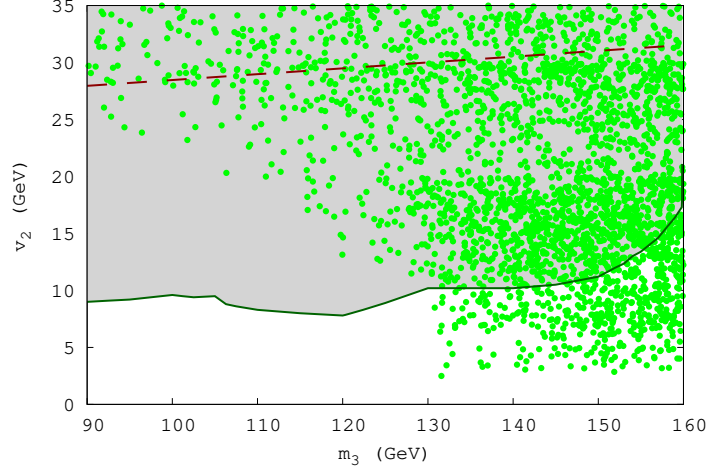


Figure 7: The allowed $m_3 - v_2$ parameter space. The theoretical constraints and the LHC Higgs signal data at $\sqrt{s} = 13$ TeV allow all the green points. The region below the dashed line (taken from [35]) are allowed by the $b \rightarrow s\gamma$ data. The gray shaded region is forbidden by the $H_3^\pm \rightarrow \tau\nu$ ATLAS data. The solid dark-green line corresponds to the $H_3^\pm \rightarrow \tau\nu$ ATLAS data for the parameter choice stated in the Eq. (24). The green points below the solid line are allowed by the theoretical constraints, LHC Higgs signal strengths at LHC $\sqrt{s} = 13$ TeV, $b \rightarrow s\gamma$ data, $H_3^\pm \rightarrow cs, \tau\nu$ ATLAS and CMS data.

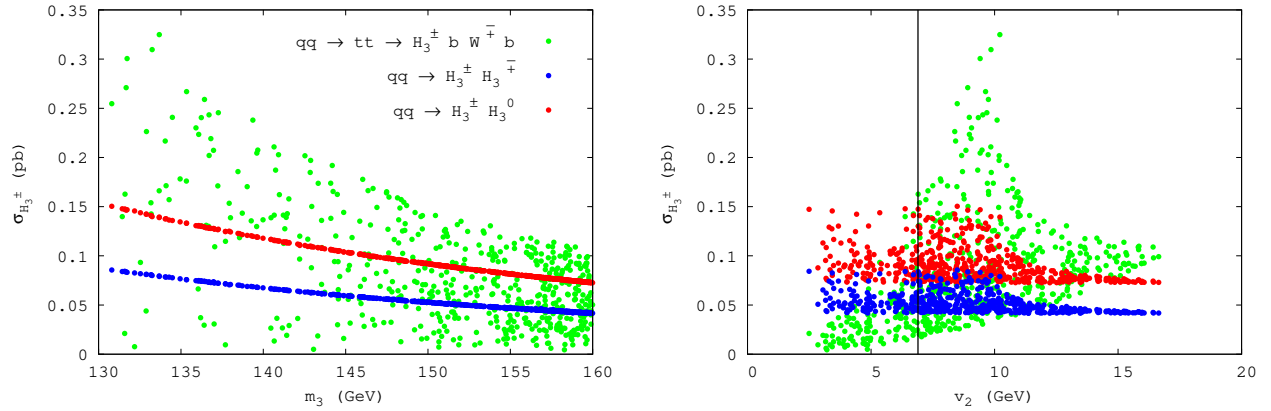


Figure 8: Production cross-sections $\sigma_{H_3^\pm}$ for (i) $qq \rightarrow tt \rightarrow H_3^\pm b W^\mp b$ (green points), (ii) $qq \rightarrow H_3^\pm H_3^\mp$ (blue points), (iii) $qq \rightarrow H_3^\pm H_3^0$ (red points) as a function of (Left) m_3 in GeV and (Right) v_2 in GeV. Color code is the same for the two plots. The black vertical line in the right figure at $v_2 \approx 7$ GeV separates two regions where the production cross-section of $qq \rightarrow tt \rightarrow H_3^\pm b W^\mp b$ is lower (left region) or greater (right region) than that of the other two processes.

and the VEVs $v_{1,2}$ also acquire limits. Now, the expressions of m_5 (Eq. 11) and m_H (Eq. 12) show that these masses depend on the λ_i s, $M_{1,2}$ and the VEVs. Therefore, fixing these parameters also puts some limits on m_5 and m_H and this can be seen from the Fig. (1).

Next, we consider the LHC data at $\sqrt{s} = 13$ TeV, which are depicted by the violet points in the plots of the Fig. (1). No limit is offered on the masses and the trilinear coefficients M_1 and M_2 by the LHC data. But, we get a prominent allowed region in the $\sin \alpha - v_2$ plane from these data, which is mainly due to the inclusion of the charged scalars in the loop for the decay channel $h \rightarrow \gamma\gamma$. If the contribution of the charged scalars H_3^\pm , H_5^\pm , and $H_5^{\pm\pm}$ are not considered in the $h \rightarrow \gamma\gamma$ decay, then we get the red points in addition to the violet points in the Fig. (1) which obey the LHC data. Mainly negative values and some small positive values (< 0.15) of $\sin \alpha$ are admitted by the LHC data. For $v_2 > 10$ GeV, no positive values of $\sin \alpha$ is allowed and for $v_2 > 20$ GeV, a further narrow region is allowed in this plane.

It should be clear from the above discussion, that, the theoretical constraints or the LHC data alone cannot curb the parameter space, and hence we are to consider both of them simultaneously, which we show in the plots of the Fig. 1 by the dark-green points. The plots in the Fig. 1 clearly admit that, though the limits on the masses (m_H, m_3, m_5) and the trilinear couplings (M_1, M_2) are mainly arising due to the adoption of the theoretical constraints, the limits on the triplet VEV v_2 and $\sin \alpha$ are direct consequence of the application of the LHC data.

4 Results

We have already mentioned that, in the GM model, there are two pairs of singly charged scalars; H_3^\pm coming from the triplet and H_5^\pm coming from the quintuplet. But, due to its pure triplet origin, H_5^\pm do not couple to the SM fermions, while H_3^\pm couple to the fermions via the doublet mixing, which can also be observed from the Eq. (10). In this paper, we are interested only in fermionic decay of the singly charged scalars, and therefore, we will talk about the branching ratios of H_3^\pm . Since we focus only on the decays of the light charged scalar, in this paper, the production process of H_3^\pm we consider is through the decay of t (or \bar{t}) to $H_3^+ b$ ($H_3^- \bar{b}$).

First, in the Fig. 2 we depict the branching ratio (BR) of $t \rightarrow H_3^+ b$ for varying v_2 and show that, for a particular mass of H_3^+ , BR increases with increasing v_2 , while it decreases with increasing mass at any fixed triplet VEV. Here, we consider three values of v_2 ; 10, 15, 20 GeV. Though the BR of the decay $t \rightarrow W^+ b$ is maximum, that of $t \rightarrow H_3^+ b$ is still sizeable in the GM model. In the Fig. 3, we show the BR of H_3^\pm as the function of mass m_3 . We only depict the decays of H_3^\pm for which the corresponding BR is greater than 0.0001. To generate these plots (Fig. 2, 3), we choose,

$$m_H = 200 \text{ GeV}, m_5 = 80 \text{ GeV}, \sin \alpha = -0.2, M_1 = M_2 = 100 \text{ GeV}, \quad (24)$$

such that, the selection of the parameters satisfy the theoretical constraints given in the Sec. 3. To plot the Fig. 3, we choose a particular value of the triplet VEV $v_2 = 20$ GeV, as the nature of this plot is independent of the value of v_2 . The plots in this Fig. 3 show that, the BR is maximum for the process $H_3^\pm \rightarrow cs$ followed by the process $H_3^\pm \rightarrow \tau^\pm \nu_\tau$ with an approximate value of 0.57 and 0.39 respectively. Therefore, we are interested in probing the parameter space of the GM model for the light (within the mass range 80 – 160 GeV) singly charged scalar H_3^\pm produced by the mechanism $t \rightarrow H_3^\pm b$, with the subsequent decays $H_3^\pm \rightarrow cs$ and $H_3^\pm \rightarrow \tau^\pm \nu_\tau$.

Light charged Higgs boson decaying via $H^\pm \rightarrow cs$ has already been searched in CMS [5] and ATLAS [6] with $\sqrt{s} = 13$ TeV. Also, search for light charged Higgs boson in the $H^\pm \rightarrow \tau^\pm \nu_\tau$ decay is already carried out in ATLAS [9] and CMS [10] with $\sqrt{s} = 13$ TeV. Though we had stringent limits on the VEV v_2 as a function of the charged Higgs mass m_{H^\pm} from the $b \rightarrow s\gamma$ decay [35], we use the experimental results from the charged Higgs decay to provide an upper limit on the triplet VEV v_2 in the GM model.

We depict $BR(t \rightarrow H_3^+ b) \times BR(H_3^+ \rightarrow c\bar{s})$ as a function of the charged scalar mass (m_3) for three choices of triplet VEV v_2 in the Fig. 4. The left plot is for CMS data and the right plot is for ATLAS data. Next, we depict the plots for the decay of H_3^\pm into $\tau^\pm\nu_\tau$ but in two different manners to apply the bound obtained from the data by ATLAS and CMS, separately. In the left plot of the Fig. 5, we show production cross section ($\sigma_{H_3^\pm}$) times branching ratio of H_3^\pm decaying into $\tau^\pm\nu_\tau$ as a function of mass m_3 in GeV, for $v_2 = 15, 20$ GeV. Following [10], we consider $\sigma_{H_3^\pm} = 2\sigma_{t\bar{t}}BR(t \rightarrow H_3^\pm b)(1 - BR(t \rightarrow H_3^\pm b))$. In the right plot of the Fig. 5, we show BR of the top quark decaying into $H_3^\pm b$ times BR of H_3^\pm decaying into $\tau^\pm\nu_\tau$ as a function of mass m_3 in GeV, for $v_2 = 10, 15, 20$ GeV. Here in the Fig. 4 and Fig. 5, the black lines represent the limits from CMS and ATLAS experiments. The shaded regions in these plots are excluded by the respective experimental data. All the points (orange and green) are allowed by the theoretical constraints and LHC Higgs data, but the orange points are forbidden by the respective experimentally observed data whereas the green points are allowed by the respective experiments. Therefore, the set of green points are different for each plot of the Fig. 4 and 5. From these decay channels, one can see that ATLAS provides a more stringent bound on the triplet VEV than CMS. Also, it can be seen that the $H_3^\pm \rightarrow \tau\nu$ decay provides a more stringent bound on v_2 than the $H_3^\pm \rightarrow cs$ decay from the ATLAS result. The $m_3 - v_2$, $m_5 - v_2$, $m_3 - m_5$, $m_H - v_2$, $v_2 - M_1$, $v_2 - M_2$, $M_1 - M_2$, $\sin\alpha - v_2$ plots in the Fig. 6 clarify this more clearly. All the points in these plots are allowed by the theoretical constraints and the LHC Higgs signal data. The gray points are excluded by the $H_3^\pm \rightarrow cs, \tau\nu$ data. The blue, red, violet, green points are allowed by the CMS $H_3^\pm \rightarrow \tau\nu$ data but the blue points are excluded by the other three experiments. The red, violet, green points are allowed by CMS $H_3^\pm \rightarrow cs$ data but the red points are excluded by the two ATLAS experiments. The violet and green points are allowed by the ATLAS $H_3^\pm \rightarrow cs$ data but the violet points are excluded by the $H_3^\pm \rightarrow \tau\nu$ ATLAS data. Only the green points survive all the above mentioned observed data. Since all the coloured points except the green points are excluded by the ATLAS $H_3^\pm \rightarrow \tau\nu$ data, one can say that among these four experimental data, the $H_3^\pm \rightarrow \tau\nu$ ATLAS data impose the most stringent constraints on the GM model parameter space.

Next, considering the parameter choice given in the Eq. (24), we varied v_2 for different m_3 and calculated $BR(t \rightarrow bH_3^\pm) \times BR(H_3^\pm \rightarrow \tau^\pm\nu)$. The solid line in the Fig. 7 corresponds to the observed data from ATLAS for this process in the GM model. The dashed line obtained from [35] for the $b \rightarrow s\gamma$ experiment was the most stringent bound on v_2 for different m_3 previously. But, the results of this paper show that the most stringent bound on v_2 for low m_3 (90 – 160 GeV) is now obtained from ATLAS data when H_3^\pm decays to $\tau\nu$. The shaded region is excluded by the ATLAS data. All the green points obey the theoretical constraints and the LHC Higgs signal strength data. Therefore, the green points above and below the solid line are forbidden and allowed by the experimental data.

In addition to the above results, this paper also compares the production cross sections of H_3^\pm ($\sigma_{H_3^\pm}$) from $t\bar{t}$ and $q\bar{q}$. Fig. 8 depicts $\sigma_{H_3^\pm}$ for (i) $qq \rightarrow tt \rightarrow H_3^\pm bW^\mp b$ (green points), (ii) $qq \rightarrow H_3^+ H_3^-$ (blue points), (iii) $qq \rightarrow H_3^\pm H_3^0$ (red points) as a function of m_3 (left) and v_2 (right). All the points in these plots are satisfied by all of the above mentioned theoretical constraints and experimentally observed data. The vertical solid line in the right plot at $v_2 \approx 7$ GeV separates two regions where the production cross-section of $qq \rightarrow tt \rightarrow H_3^\pm bW^\mp b$ is lower (left region) or greater (right region) than that of the other two production processes. The solid line indicating the upper limit on v_2 as a function of low m_3 in the Fig. 7 shows that the minimum value of the allowed upper limit is always greater than 7 GeV and hence we can safely consider the production cross section of H_3^\pm from the top (anti)quark decay instead of the DrellYan processes as depicted in the Fig. 8.

To generate the plots, we first implement the model in Feynrules [48] to obtain the UFO file required to generate events using MadGraph5 (v2.8.2) [49].

5 Conclusions

Recent searches at the LHC for light singly-charged scalar decaying into either cs or $\tau^\pm\nu_\tau$ encourage us to investigate these decay channels in BSM model with triplets. We choose the Georgi-Machacek model, where the scalar sector of SM is added by a real and a complex triplet, such that, the custodial symmetry is preserved at the tree level. Besides two doubly charged scalars, there are four singly-charged scalars in this model, out of which two (H_5^\pm) do not have any couplings with the SM fermions. Therefore, we are interested in the production and decay of the other two singly-charged scalars (H_3^\pm). Since, we consider only the decay of light charged scalars, within the mass range of 80 – 160 GeV, the production mechanism we contemplate is $t \rightarrow H_3^\pm b$, though we compared the production processes of $qq \rightarrow tt \rightarrow H_3^\pm b W^\mp b$ with that of $qq \rightarrow H_3^+ H_3^-$ and $qq \rightarrow H_3^\pm H_3^0$. We get an upper bound on the triplet VEV by considering the experimental limits provided by ATLAS and CMS at the LHC with $\sqrt{s} = 13$ TeV, for the decay channels $H_3^\pm \rightarrow cs$ and $H_3^\pm \rightarrow \tau^\pm\nu_\tau$, separately. The strongest bound is coming from the $H_3^\pm \rightarrow \tau^\pm\nu_\tau$ decay observed by ATLAS. On top of this, we also considered the restrictions on the parameter space arising from the theoretical constraints and Higgs data. We showed that, simultaneous adoption of these constraints also curb the parameter space of the GM model.

Acknowledgements — The author would like to acknowledge the SERB grant CRG/2018/004889 as an honorary fellow without any financial support and Department of Science and Technology, Government of India for financial support through SERB-NPDF scholarship with grant no. PDF/2022/001784. SG also thanks Prof. Anirban Kundu for useful discussions and Dr. Suman Chatterjee for technical help in MadGraph5.

References

- [1] G. Aad *et al.* [ATLAS], Phys. Lett. B **716**, 1-29 (2012) doi:10.1016/j.physletb.2012.08.020 [arXiv:1207.7214 [hep-ex]].
- [2] S. Chatrchyan *et al.* [CMS], Phys. Lett. B **716**, 30-61 (2012) doi:10.1016/j.physletb.2012.08.021 [arXiv:1207.7235 [hep-ex]].
- [3] A. Ivina [ATLAS], PoS **EPS-HEP2021**, 631 (2022) doi:10.22323/1.398.0631
- [4] [ATLAS], ATLAS-CONF-2021-037.
- [5] A. M. Sirunyan *et al.* [CMS], Phys. Rev. D **102**, no.7, 072001 (2020) doi:10.1103/PhysRevD.102.072001 [arXiv:2005.08900 [hep-ex]].
- [6] G. Aad *et al.* [ATLAS], [arXiv:2407.10096 [hep-ex]].
- [7] G. Aad *et al.* [ATLAS], Eur. Phys. J. C **73**, no.6, 2465 (2013) doi:10.1140/epjc/s10052-013-2465-z [arXiv:1302.3694 [hep-ex]].
- [8] [ATLAS], ATL-PHYS-PUB-2010-006.
- [9] M. Aaboud *et al.* [ATLAS], JHEP **09**, 139 (2018) doi:10.1007/JHEP09(2018)139 [arXiv:1807.07915 [hep-ex]].
- [10] A. M. Sirunyan *et al.* [CMS], JHEP **07**, 142 (2019) doi:10.1007/JHEP07(2019)142 [arXiv:1903.04560 [hep-ex]].
- [11] S. Abbaspour, S. M. Moosavi Nejad and M. Balali, Nucl. Phys. B **932**, 505-528 (2018) doi:10.1016/j.nuclphysb.2018.05.023 [arXiv:1806.02546 [hep-ph]].

- [12] M. Aaboud *et al.* [ATLAS], Phys. Lett. B **759**, 555-574 (2016) doi:10.1016/j.physletb.2016.06.017 [arXiv:1603.09203 [hep-ex]].
- [13] [ATLAS], ATLAS-CONF-2011-151.
- [14] G. Aad *et al.* [ATLAS], JHEP **06**, 039 (2012) doi:10.1007/JHEP06(2012)039 [arXiv:1204.2760 [hep-ex]].
- [15] A. Ali, F. Barreiro and J. Llorente, Eur. Phys. J. C **71**, 1737 (2011) doi:10.1140/epjc/s10052-011-1737-8 [arXiv:1103.1827 [hep-ph]].
- [16] S. Chatrchyan *et al.* [CMS], JHEP **07**, 143 (2012) doi:10.1007/JHEP07(2012)143 [arXiv:1205.5736 [hep-ex]].
- [17] K. Cheung, A. Jueid, J. Kim, S. Lee, C. T. Lu and J. Song, [arXiv:2201.06890 [hep-ph]].
- [18] G. Abbiendi *et al.* [ALEPH, DELPHI, L3, OPAL and LEP], Eur. Phys. J. C **73**, 2463 (2013) doi:10.1140/epjc/s10052-013-2463-1 [arXiv:1301.6065 [hep-ex]].
- [19] A. G. Akeroyd, M. Aoki, A. Arhrib, L. Basso, I. F. Ginzburg, R. Guedes, J. Hernandez-Sanchez, K. Huitu, T. Hurth and M. Kadastik, *et al.* Eur. Phys. J. C **77**, no.5, 276 (2017) doi:10.1140/epjc/s10052-017-4829-2 [arXiv:1607.01320 [hep-ph]].
- [20] R. Benbrik, M. Boukidi, B. Manaut, M. Ouchemhou, S. Semlali and S. Taj, [arXiv:2112.07502 [hep-ph]].
- [21] A. G. Akeroyd, S. Moretti, K. Yagyu and E. Yildirim, Int. J. Mod. Phys. A **32**, no.23n24, 1750145 (2017) doi:10.1142/S0217751X17501457 [arXiv:1605.05881 [hep-ph]].
- [22] A. G. Akeroyd, S. Moretti and J. Hernandez-Sanchez, Phys. Rev. D **85**, 115002 (2012) doi:10.1103/PhysRevD.85.115002 [arXiv:1203.5769 [hep-ph]].
- [23] A. G. Akeroyd, S. Moretti and M. Song, [arXiv:2202.03522 [hep-ph]].
- [24] W. S. Hou, R. Jain and T. Modak, [arXiv:2111.06523 [hep-ph]].
- [25] A. G. Akeroyd, S. Moretti and M. Song, Phys. Rev. D **101**, no.3, 035021 (2020) doi:10.1103/PhysRevD.101.035021 [arXiv:1908.00826 [hep-ph]].
- [26] A. G. Akeroyd, S. Moretti and M. Song, Phys. Rev. D **98**, no.11, 115024 (2018) doi:10.1103/PhysRevD.98.115024 [arXiv:1810.05403 [hep-ph]].
- [27] H. Georgi and M. Machacek, Nucl. Phys. B **262**, 463-477 (1985) doi:10.1016/0550-3213(85)90325-6
- [28] N. Ghosh, S. Ghosh and I. Saha, Phys. Rev. D **101**, no.1, 015029 (2020) doi:10.1103/PhysRevD.101.015029 [arXiv:1908.00396 [hep-ph]].
- [29] H. E. Logan and Y. Wu, JHEP **11**, 121 (2018) doi:10.1007/JHEP11(2018)121 [arXiv:1809.09127 [hep-ph]].
- [30] A. Ismail, H. E. Logan and Y. Wu, [arXiv:2003.02272 [hep-ph]].
- [31] K. Hartling, K. Kumar and H. E. Logan, Phys. Rev. D **90**, no.1, 015007 (2014) doi:10.1103/PhysRevD.90.015007 [arXiv:1404.2640 [hep-ph]].
- [32] M. E. Krauss and F. Staub, Eur. Phys. J. C **78**, no.3, 185 (2018) doi:10.1140/epjc/s10052-018-5676-5 [arXiv:1709.03501 [hep-ph]].

- [33] G. Moultaqa and M. C. Peyranère, Phys. Rev. D **103**, no.11, 115006 (2021) doi:10.1103/PhysRevD.103.115006 [arXiv:2012.13947 [hep-ph]].
- [34] M. Aoki and S. Kanemura, Phys. Rev. D **77**, no.9, 095009 (2008) [erratum: Phys. Rev. D **89**, no.5, 059902 (2014)] doi:10.1103/PhysRevD.77.095009 [arXiv:0712.4053 [hep-ph]].
- [35] K. Hartling, K. Kumar and H. E. Logan, Phys. Rev. D **91**, no.1, 015013 (2015) doi:10.1103/PhysRevD.91.015013 [arXiv:1410.5538 [hep-ph]].
- [36] J. Chang, C. R. Chen and C. W. Chiang, JHEP **03**, 137 (2017) doi:10.1007/JHEP03(2017)137 [arXiv:1701.06291 [hep-ph]].
- [37] C. W. Chiang and T. Yamada, Phys. Lett. B **735**, 295-300 (2014) doi:10.1016/j.physletb.2014.06.048 [arXiv:1404.5182 [hep-ph]].
- [38] R. Zhou, W. Cheng, X. Deng, L. Bian and Y. Wu, JHEP **01**, 216 (2019) doi:10.1007/JHEP01(2019)216 [arXiv:1812.06217 [hep-ph]].
- [39] A. Banerjee, G. Bhattacharyya and N. Kumar, Phys. Rev. D **99**, no.3, 035028 (2019) doi:10.1103/PhysRevD.99.035028 [arXiv:1901.01725 [hep-ph]].
- [40] C. W. Chiang, S. Kanemura and K. Yagyu, Phys. Rev. D **90**, no.11, 115025 (2014) doi:10.1103/PhysRevD.90.115025 [arXiv:1407.5053 [hep-ph]].
- [41] C. W. Chiang, S. Kanemura and K. Yagyu, Phys. Rev. D **93**, no.5, 055002 (2016) doi:10.1103/PhysRevD.93.055002 [arXiv:1510.06297 [hep-ph]].
- [42] H. E. Logan and V. Rentala, Phys. Rev. D **92**, no.7, 075011 (2015) doi:10.1103/PhysRevD.92.075011 [arXiv:1502.01275 [hep-ph]].
- [43] A. Kundu, P. Mondal and P. B. Pal, [arXiv:2111.14195 [hep-ph]].
- [44] K. Hartling, K. Kumar and H. E. Logan, [arXiv:1412.7387 [hep-ph]].
- [45] C. W. Chiang, G. Cottin and O. Eberhardt, Phys. Rev. D **99**, no.1, 015001 (2019) doi:10.1103/PhysRevD.99.015001 [arXiv:1807.10660 [hep-ph]].
- [46] [CMS], CMS-PAS-HIG-17-031.
- [47] [ATLAS], ATLAS-CONF-2019-005.
- [48] A. Alloul, N. D. Christensen, C. Degrande, C. Duhr and B. Fuks, Comput. Phys. Commun. **185**, 2250-2300 (2014) doi:10.1016/j.cpc.2014.04.012 [arXiv:1310.1921 [hep-ph]].
- [49] J. Alwall, R. Frederix, S. Frixione, V. Hirschi, F. Maltoni, O. Mattelaer, H. S. Shao, T. Stelzer, P. Torrielli and M. Zaro, JHEP **07**, 079 (2014) doi:10.1007/JHEP07(2014)079 [arXiv:1405.0301 [hep-ph]].